Disentangling cortical functional connectivity strength and topography reveals divergent roles of genes and environment

Bianca Burger, Karl-Heinz Nenning, Ernst Schwartz, Daniel S Margulies, Alexandros Goulas, Hesheng Liu, Simon Neubauer, Justin Dauwels, Daniela Prayer, Georg Langs

NeuroImage 247 (2022) 118770

Contents lists available at ScienceDirect

NeuroImage

journal homepage: www.elsevier.com/locate/neuroimage

Disentangling cortical functional connectivity strength and topography reveals divergent roles of genes and environment

Bianca Burger[a], Karl-Heinz Nenning[a,b], Ernst Schwartz[a], Daniel S. Margulies[c,d], Alexandros Goulas[e], Hesheng Liu[f], Simon Neubauer[g], Justin Dauwels[h,i], Daniela Prayer[j], Georg Langs[a,k,*]

[a] Department of Biomedical Imaging and Image-Guided Therapy, Computational Imaging Research Lab, Medical University of Vienna, Vienna 1090, Austria
[b] Center for Biomedical Imaging and Neuromodulation, Nathan Kline Institute, Orangeburg, NY, United States
[c] Université de Paris, CNRS, Integrative Neuroscience and Cognition Center, 75006 Paris, France
[d] Wellcome Centre for Integrative Neuroimaging, Nuffield Department of Clinical Neurosciences, University of Oxford, Oxford OX3 9DU, United Kingdom
[e] Institute for Computational Neuroscience, University Medical Center Hamburg-Eppendorf, Hamburg University, Martinstr. 52, 20246 Hamburg, Germany
[f] Department of Neuroscience, Medical University of South Carolina, Charleston, SC, 29466, USAs
[g] Department of Human Evolution, Max Planck Institute for Evolutionary Anthropology, Leipzig 04103, Germany
[h] TU Delft Fac. EEMCS Mekelweg 4 2628 CD Delft
[i] Nayang Technological University, 639798, Singapore
[j] Department of Biomedical Imaging and Image-Guided Therapy, Division of Neuroradiology and Musculo-skeletal Radiology, Medical University of Vienna, Vienna 1090, Austria
[k] Computer Science and Artificial Intelligence Laboratory, Massachusetts Institute of Technology, Cambridge, MA 02139, United States

ARTICLE INFO

Keywords:
inter-subject variability
heritability
functional magnetic resonance imaging
functional connectivity
topography

ABSTRACT

The human brain varies across individuals in its morphology, function, and cognitive capacities. Variability is particularly high in phylogenetically modern regions associated with higher order cognitive abilities, but its relationship to the layout and strength of functional networks is poorly understood. In this study we disentangled the variability of two key aspects of functional connectivity: strength and topography. We then compared the genetic and environmental influences on these two features. Genetic contribution is heterogeneously distributed across the cortex and differs for strength and topography. In heteromodal areas genes predominantly affect the topography of networks, while their connectivity strength is shaped primarily by random environmental influence such as learning. We identified peak areas of genetic control of topography overlapping with parts of the processing stream from primary areas to network hubs in the default mode network, suggesting the coordination of spatial configurations across those processing pathways. These findings provide a detailed map of the diverse contribution of heritability and individual experience to the strength and topography of functional brain architecture.

1. Introduction

Evolution has shaped the cortical layout of the human brain through both scaling and reorganization (Smaers and Soligo, 2013). The typical globular shape of the brain evolved gradually within Homo sapiens in the last 300,000 years (Neubauer et al., 2018) and has been linked to genes associated with neurogenesis and myelination (Gunz et al., 2019). This is related to the evolution of a developmental globularization of the brain in the first year of life, which does not occur in our closest living relatives, the chimpanzees (Neubauer et al., 2010), nor in our closest extinct relatives, the Neanderthals (Gunz et al., 2010). It is during this developmental period that the human brain is more susceptible to environmental influence. Modern humans have more neurocranial shape variation than Neanderthals and other archaic Homo groups (Gunz et al., 2009). A remarkable feature of the brain is that evolutionary selection and adaptation result not in a static organ, but in the

Abbreviations: aFC, variability of functional connectivity before disentanglement; SP, variability of topography of corresponding functional regions; FC, variability of functional connectivity strength of corresponding functional regions; AaFC, ASP, AFC, genetic contribution to indicated type of variability; EaFC, ESP, EFC, random environmental contribution to indicated type of variability.

* Corresponding author at: Department of Biomedical Imaging and Image-guided Therapy, Computational Imaging Research Lab, Medical University of Vienna, Vienna 1090, Austria.
E-mail address: georg.langs@meduniwien.ac.at (G. Langs).

https://doi.org/10.1016/j.neuroimage.2021.118770.
Received 4 August 2021; Received in revised form 10 November 2021; Accepted 29 November 2021
Available online 30 November 2021.

capability to adapt to the environment during the life-long process of development and learning (Krubitzer and Prescott, 2018). The increased variability of functional brain architecture across individuals is associated with both differences in genetic programming and individual experience.

This variability is not evenly distributed across the brain. For instance, areas in the prefrontal cortex and association areas exhibit particularly high inter-individual differences in functional architecture (Mueller et al., 2013; Nenning et al., 2017). These areas are notable for exhibiting a predominance of long-range connectivity (Sepulcre et al., 2010) as well as evolutionarily recent expansion (Mueller et al., 2013). The link between these observations is subject to different hypotheses (Mueller et al., 2013; Buckner and Krienen, 2013). Inter-subject variability might be associated with the potential for architectural alternatives at different locations but with comparable capacity. It appears to be linked with plasticity and the corresponding recovery of patients suffering from focal brain damage (Seghier and Price, 2018). Differences in individual experience may contribute to measurable diversity as well. Inter-subject variability in preterm neonates and healthy adults exhibit overall similar patterns (Stoecklein et al., 2020), but variability increases for parts of the fronto-parietal and dorsal attention network during maturation. At the same time, genes contribute significantly to the variability of functional (Colclough et al., 2017; Reineberg et al., 2019), and structural (Shen et al., 2014; Xie et al., 2018) cortical networks.

Despite the evidence for both genetic and environmental influences on brain variability, their specific contributions to variability of two key features of functional organization — strength and topography — remain poorly understood. Both, variability of topography or spatial layout and connectivity strength is present across subjects (Nenning et al., 2017). Therefore we only observe a mixture of both when variability in anatomically aligned subjects is measured (Mueller et al., 2013).

In this study, we disentangled variability of the connectivity *strength* between components of functional networks and the spatial cortical layout of these nodes - their *topography* - to study independent contributions of genetics and environment (e.g., learning, experience) to variability of these two features. We analysed resting state functional magnetic resonance imaging (rs-fMRI) data of twins. To disentangle strength and topography, we first performed cortical registration based on anatomical features, and then identified variability of topography by subsequent functional registration. We found that the cortical landscapes of genetic influence on variability of these two features diverge along an axis from primary to higher order association areas. In primary areas variability of connectivity strength exhibits high heritability compared to topography, while this relationship is reversed in parts belonging to association areas. Distinguishing the role of individual experience in shaping variation of connectivity strength from the role of heritability in shaping its topographical variability may provide crucial insights into the mechanisms enabling the flexible, yet stable nature of brain organization supporting the human cognitive repertoire.

2. Material & methods

2.1. Dataset and preprocessing

We use the data of 231 participants labeled either as monozygotic or dizygotic twin taken from the HCP S1200 ICA-FIX denoised dataset. Only twins with 4 rsfMRI runs available are chosen. Although not intended on purpose, there were then only same-sex dizygotic twin pairs included in the study. Further details on exclusion criteria and data acquisition are described elsewhere (Van Essen et al., 2012, 2013; Dubois et al., 2018; Uğurbil et al., 2013). 112 subjects out of 231 are labeled as monozygotic twin. The mean age in this group is 30.02 years and 74% are female. The group of monozygotic twins consists of 2 subjects denoted as “Asian/Nat. Hawaiian/Other Pacific”, 12 denoted as “Black or African Am”, 1 as “Unknown or Not Reported and 97 as “White”. The other 119 subjects labeled as dizygotic are 62% female an the mean age in this group is 29.82 years. 4 are denoted as “Asian/Nat. Hawaiian/Other Pacific”, 21 as “Black or African Am”, 1 as “Unknown or Not Reported and 93 as “White”. Participants provided verbal consent in accordance with guidelines set by the Wu-Minn HCP Consortium.

The preprocessing consists of the HCP-pipelines (Glasser et al., 2013), which include processing of the volume data and bringing the participant’s surface into a standard space (fs_LR). For the ICA-FIX dataset independent component analysis is used to decompose the data set into “good” and “bad” components based on the volume data. Bad components are then removed from the surface data (Griffanti et al., 2014; Salimi-Khorshidi et al., 2014). Global signal regression and band-pass filtering (range 0.01 Hz–0.08 Hz) are applied in addition to the HCP-pipelines. Furthermore, the fMRI time-series are mapped to Freesurfer’s (Fischl et al., 1999) fsaverage4 (version 5.3) surface using Connectome Workbench v1.3 (Marcus et al., 2013). In the following sections, we explain the methodology used to disentangle functional connectivity strength and topography and estimate genetic and environmental influence on their variability. Supplementary Figure 1 gives an overview of the processing flow.

2.2. Decoupling function from anatomy

To independently investigate the genetic- and environmental contribution to variability of functional connectivity and its spatial topography across the cortex, we first disentangle these two components (Fig. 1a). After anatomical alignment of cortical surfaces of all individuals (Glasser et al., 2013), we embed the cortical functional connectivity structure into a representational space, and align functional networks in this space (Margulies et al., 2016; Langs et al., 2014). To obtain the embedding, diffusion maps are used (Nenning et al., 2017; Coifman and Lafon, 2006). For our study we focused on functional intersubject variability in resting state fMRI, therefore we used only functional resting state features given through the gradients for alignment instead of the multimodal approach (Glasser et al., 2016; Robinson et al., 2014). For each twin a correlation matrix including all vertices of the left and right hemisphere is calculated. As in Margulies et al. (Margulies et al., 2016) the cosine similarity metric is applied to each pair of rows of an individual’s correlation matrix and based on the obtained values, a new symmetric similarity $\mathbf{W}$ is constructed for the participant in which the entries correspond to the cosine similarity value of the row pairs of the individual’s correlation matrix. Since the cosine similarity gives values between -1 and 1, the range of the entries of $\mathbf{W}$ is shifted so that the largest value is 2 and all entries are larger than 0. The matrix $\mathbf{W}$ of each individual then represents the edge weights of a similarity graph. Compared to Margulies et al. (2016) who first calculated a correlation matrix based on fMRI time series and thresholded it before applying the cosine similarity, we did not want to discard information through thresholding. To obtain non-negative affinity matrix entries for diffusion map calculation we shifted all values into the range 0–2, to represent the relationships among node pairs. We interpreted the decreasing values of the cosine similarity or the correspondingly increasing angle between two nodes as an increase in difference between those nodes. A shift of values into the range 0–2 therefore still represents a valid relationship among nodes.

The next step is obtaining a spectral representation of the connectivity structure via eigendecomposition of the matrix $\mathbf{L}=\check{\mathbf{C}}^{-1}(\mathbf{D}^{-1/2}\mathbf{W}\mathbf{D}^{-\frac{1}{2}})$, where $\mathbf{D}$ is the diagonal matrix of node degrees $d_i=\Sigma_j(\mathbf{W}_{i,j})$ and $\check{\mathbf{C}}$ is the diagonal matrix of node degrees $\check{c}_i=\Sigma_j(\mathbf{D}^{-1/2}\mathbf{W}\mathbf{D}^{-\frac{1}{2}})_{i,j}$. We basically apply graph laplacian normalization to $\mathbf{D}^{-1/2}\mathbf{W}\mathbf{D}^{-\frac{1}{2}}$ (Coifman and Lafon, 2006). Embedding coordinates Ψ_i of vertex i are derived from the right eigenvectors of $\mathbf{L}$ multiplied with $\lambda_k/(1-\lambda_k)$, where λ_k denotes the eigenvalue of the k^{th} eigenvector ψ_k, as

$$\Psi_i = \left(\psi_1(i), \psi_2(i), \ldots, \psi_N(i)\right)^T$$

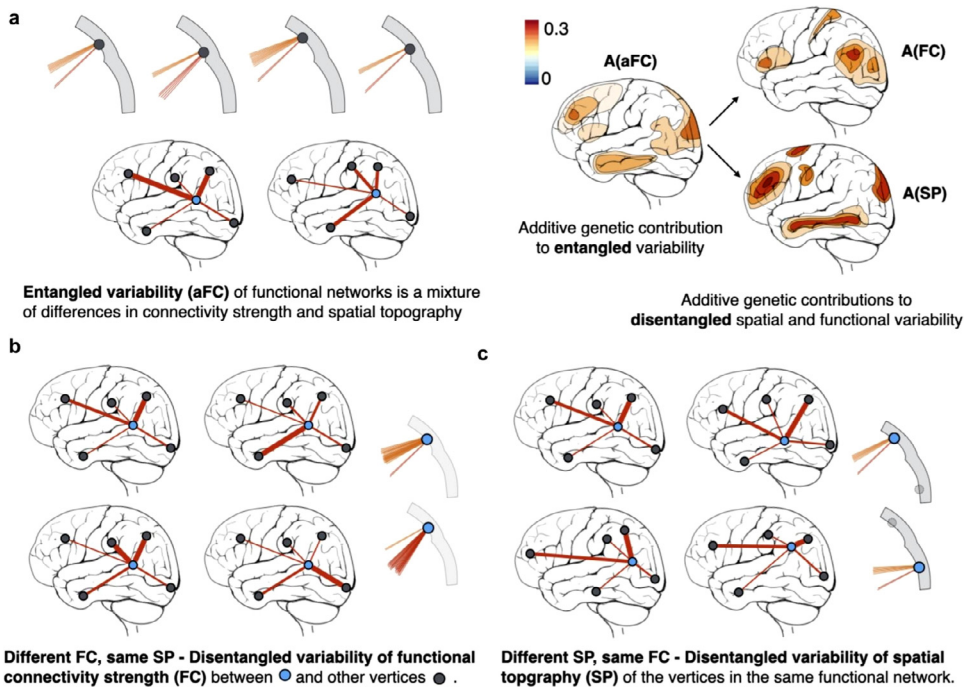

Fig. 1. Overview. (a) Disentangling functional connectivity and topography of functionally corresponding units on the cortex enables the independent analysis of genetic contributions to these different features of variability. (b) After disentanglement, FC captures variability of connectivity strength of corresponding network nodes regardless of their spatial variability. In each of the four exemplary brains, the strength of connections is represented by the thickness of connecting lines. (c) SP is the variability of the spatial position (topography) of functionally corresponding vertices. When subjects are anatomically aligned, functional corresponding units or vertices (the blue vertex in the bottom right panel) differ in spatial position (coordinates). To know which units are functionally corresponding across subjects we perform functional alignment. (For interpretation of the references to color in this figure legend, the reader is referred to the web version of this article.)

$\psi_1(i)$ is the i^{th} entry of the first eigenvector.

In order to reach functional correspondence across participants the embedding of each twin $\Psi^S = (\psi_1{}^S, \psi_2{}^S, \ldots, \psi_N{}^S)$ is aligned to the embedding $\Psi^R = (\psi_1{}^R, \psi_2{}^R, \ldots, \psi_N{}^R)$ of a reference participant (ID: 101915) not part of the twin dataset by calculating a rotation matrix $\mathbf{Q_{S,R}}$, that has the form

$$\mathbf{Q_{S,R}} = \mathbf{VU}^T,$$

with $\mathbf{V}$ and $\mathbf{U}$ constructed via singular value decomposition,

$$U\Sigma V^T = \left(\Psi^R\right)^T \Psi^S.$$

A publically available implementation is used to obtain and align diffusion maps (mapalign: https://github.com/satra/mapalign). Our obtained gradients 1, 2 and 3 are comparable to Margulies' gradients 1, 3, and 4, separating visual/somatomotor and default mode network, frontoparietal/attention networks and default mode networks, and visual cortex and regions belonging to task positive networks, respectively. After having obtained the embedding coordinates the first three are used as features for surface registration with MSM v2 (Robinson et al., 2014, 2018; Ishikawa, 2014), where each twin's surface is aligned to the reference surface. We used only the first 3 components for alignment because after the third embedding coordinate the eigenvalues of the remaining coordinates decreased more continuously, indicating a worse separation from each other. Beside, we also followed Nenning et al. (2015) who used diffusion maps for multi-subject functional registration and found that using the first 3 components gave the best results. Box plots summarizing the distribution of eigenvalues across subjects for the first 7 components are shown in Supplementary Fig. 2. Deformation fields for discovery and robustness analysis are shown in Supplementary Fig. 3. After alignment a vertex of the twin is assigned to each vertex of the reference participant, using nearest neighbor to reach functional correspondence of vertices across all individuals in the twin dataset. $\mathbf{W}$ can be constructed in different ways from the signal correlation data. To investigate the stability of the gradients dependent on the construction of $\mathbf{W}$, we also calculated gradients by (1) thresholding $\mathbf{W}$ at 0 and (2) taking the absolute values $\mathbf{W}$ instead of shifting the range. Supplementary Fig. 4 shows the first 3 gradients for shifted, thresholded and absolute $\mathbf{W}$. For the first two variants, gradients are qualitatively similar despite different constructions of $\mathbf{W}$.

This functional alignment allows us to observe variability in the spatial position - *topography* - of corresponding functional regions (SP) and variability of functional connectivity strength of these corresponding functional regions (FC) independently (Fig. 1b). More details on quantification of variability of connectivity strength or topography are found in the next section. Calculations in this manuscript are performed with Python 3.6, if not stated otherwise.

2.3. Parcellation and quantification of inter-subject variability

After preprocessing the cortex is parceled into 600 parts, 300 per hemisphere, using the Schaefer – 600 parcellation scheme (Schaefer et al., 2018). The advantage of this scheme is the possibility to assign each region of interest (ROI) to one of the 7 Yeo-networks (Yeo et al., 2011). In this study the networks are split into a left and a right part yielding 14 networks. For each of the 14 networks a representative ROI is chosen by correlating first each ROI time series of a network with all the other time series of the same network. The ROI with the highest mean correlation value is then chosen as the representative ROI for each of the 14 networks. For this purpose the concatenated LR-Runs 1 and 2 are used. The choice of the representative ROIs is done based on the reference subject and then taken over for all participants.

Using the representative ROIs we construct connectivity profiles of size 1×13 for each vertex of the cortex and subject by calculating the Pearson correlation coefficients between the time series of the current vertex under investigation and the 13 representative ROIs of the networks to which the current vertex does not belong. This is done for anatomically aligned subjects, as well as, after functional alignment. The connectivity profiles for each vertex describe the corresponding variability across subjects of entangled functional connectivity and disentangled connectivity strength, respectively, and serve as phenotype description for the twin model. A Fisher's z transformation is applied afterwards and gender as well as the mean relative root mean squared motion difference of Run 1 and 2 are regressed out. Age was not included as a regressor since all subjects are young adults with age raging from 22 to 36, similar as in Reineberg et al. (2019). The regression is done using *R* version 3.4.

To describe the phenotype or variation of spatial layout, each functionally corresponding vertex of each participant is described by its orig-

inal position in 3-dimensional space before functional alignment. This captures the variability of the observed cortical positions of nodes in the functional networks that were brought into correspondence by functional alignment, since their connectivity profiles were similar. Then the twin model used is the same as for connectivity strength, the only difference is that the phenotype of each participant is described by 3 traits instead of 13.

2.4. ACE twin model

To obtain estimates for the genetic and environmental influences on the variability of connectivity strength or position of each vertex, we use multivariate twin models (Neale and Maes, 2021). We analyze additive genetic (A), common environmental (C), and random environmental (E) factors on these two types of variability. To enable comparison of results with prior work, we also analyze these factors for functional connectivity before disentanglement (aFC). This reflects the combined variability of topography and connectivity strength at any cortical position. In the model for connectivity strength the phenotype of each vertex and individual is described by 13 character traits, namely the correlation with the representative ROIs. For variability of position 3 character traits are used for description, namely the 3-dimensional original (prior to functional alignment) coordinates of functionally corresponding vertices. The model is applied to each vertex separately and the relation between these character traits is summarized in the expected population covariance matrix $\mathbf{V}_p$. It can be split into three covariances representing the additive genetic influence **A**, the common environmental influence **C** and the random environmental influence **E**, i.e.

$$\mathbf{V}_p = \mathbf{A} + \mathbf{C} + \mathbf{E}.$$

$\mathbf{V}_p$, **A, C** and **E** are of dimension 13×13 or 3×3, respectively. Additive genetic control refers to the additive effects of the two variants of a gene (allele) present in a human being. The two alleles can interact with each other leading to non-additive interaction effects. The typically larger additive genetic contribution together with non-additive interaction effects comprise the total genetic contribution (Bürger, 2000). The common environment **C** makes members of the same family more similar to each other than to members of different families. The random environment **E** causes the differences between members of the same family. To ensure that the estimated matrices **A, C** and **E** are symmetric and positive definite, they are written as a Cholesky decomposition, $\mathbf{A}=\mathbf{T}_A\mathbf{T}_A{}^T$, $\mathbf{C}=\mathbf{T}_C\mathbf{T}_C{}^T$, $\mathbf{E}=\mathbf{T}_E\mathbf{T}_E{}^T$, with lower triangular matrices $\mathbf{T}_A$,$\mathbf{T}_C$ and $\mathbf{T}_E$.

To obtain estimates for $\mathbf{T}_A$,$\mathbf{T}_C$ and $\mathbf{T}_E$ the expected trait covariance structure of monozygotic and dizygotic twin pairs is used. It can be shown that the covariance matrices for monozygotic $\mathbf{V}_{MZ}$ and dizygotic twins $\mathbf{V}_{DZ}$ are given by the block matrices,

$$\mathbf{V}_{MZ} = \begin{pmatrix} \mathbf{A}+\mathbf{C}+\mathbf{E} & \mathbf{A}+\mathbf{C} \\ \mathbf{A}+\mathbf{C} & \mathbf{A}+\mathbf{C}+\mathbf{E} \end{pmatrix},$$

$$\mathbf{V}_{DZ} = \begin{pmatrix} \mathbf{A}+\mathbf{C}+\mathbf{E} & 0.5\mathbf{A}+\mathbf{C} \\ 0.5\mathbf{A}+\mathbf{C} & \mathbf{A}+\mathbf{C}+\mathbf{E} \end{pmatrix}.$$

$\mathbf{V}_{MZ}$ and $\mathbf{V}_{DZ}$ are of dimensions 26×26 for connectivity strength and 6×6 for position variability. This means that the trait covariance of a twin (monozygotic, as well as dizygotic) with himself is $\mathbf{A} + \mathbf{C} + \mathbf{E}=\mathbf{V}_p$. The trait covariance of monozygotic Twin 1 with Twin 2 is $\mathbf{A} + \mathbf{C}$, whereas for dizygotic twin pairs it is $0.5\mathbf{A}+\mathbf{C}$, since they share on average only half of their genes, whereas the genes of monozygotic twins are identical. For parameter estimation the expected trait population covariance matrix $\mathbf{V}_p$, as well as the expected covariances of Twin 1 with Twin 2 (mono- and dizygotic) are then equated with the corresponding values calculated from the dataset. The twin model is implemented using R's package OpenMx version 2.11.5 (Neale et al., 2016; Hunter, 2018).

2.5. Analysis

After estimation, genetic, common environmental and random environmental contribution maps are available for variability of connectivity strength after anatomical and functional alignment and for the spatial layout. Note that values for A, C and E are only considered for vertices with corresponding fMRI signal and which can be assigned to one of the 600 ROIs (2339/2562 vertices on the left and 2341/2562 on the right hemisphere). This excludes mainly vertices from the medial wall. Several comparisons are made. First, the genetic contributions to variability in connectivity strength after anatomical and functional alignment are compared to each other by comparing the mean genetic contribution on the surface using a paired *t*-test. The normality assumption for the differences of paired values is verified using a histogram (Supplementary Fig. 5). Additionally, the genetic contributions to variability of connectivity strength before and after functional alignment and to spatial layout are correlated with each other using Pearson's correlation coefficient. Furthermore, the genetic contributions to variability of the spatial layout are correlated with variability in spatial layout, distance to primary area and cortex expansion. Uncorrected and corrected *p*-values are provided for the correlation coefficients and the *t*-test, whereas the uncorrected *p*-values for correlation coefficients are calculated with a spin test using 10,000 spins in Matlab (Alexander-Bloch et al., 2018). The level of significance is set to 0.05 and obtained *p*-values are adjusted through Holm-Bonferroni-correction. Holm-Bonferroni correction is done for each hemisphere separately and covers the *t*-test and correlation of heritability of SP with variability in spatial layout, distance to primary area and cortex expansion as well as correlations between genetic contributions to variability of connectivity strength before and after functional alignment and to spatial layout with each other. Correlations between heritability of SP and FC with corresponding test-retest maps are also included in the multi-comparisons correction procedure (compare Limitations section).

We also investigated the relation between function and heritability as presented in Figs. 4 and 5. In Fig. 4 we find the vertices with heritability estimates as estimated by the twin model belonging to the top 20% and bottom 20%. Then we get the density of points for bottom and top 20% in functional gradient space (Margulies et al., 2016) separately. Finally we take the difference of densities and plot it with blue indicating bottom 20% dominance and red indicating top 20% dominance. In Fig. 5 values of genetic contribution to FC (A_{FC}) and SP (A_{SP}) are divided into 10 bins based on percentiles (*x*-axis). Within each bin normalized activation probabilities are summed given one of 12 components related to function (i.e. language) (Yeo et al., 2016). The 12 components (rows) are ordered based on the difference of activation probabilities between A_{FC} and A_{PS} summed over bins and weighted by the log of percentile. The sequence visualizes the gradient from high A_{SP} and low A_{FC} on top, towards low A_{SP} and high A_{FC} on the bottom. The 12 activation probability maps and the maps for A_{FC} and A_{SP} are in the same space, therefore activation probabilities of voxels lieing in one A_{SP}/A_{FC} -bin can be summed.

Additionally we performed robustness analysis using 2 RL fMRI runs, which have also been available for each participant additionally to the 2 LR runs used for the discovery analysis. In addition to performing the same steps as described in the first paragraph of this section, we also correlated maps based on the discovery dataset with maps obtained based on the RL runs. Note that for each category either aFC, FC or SP there were some vertices for which an optimal solution for the estimates of the twin model could not be found. This holds for the robustness as well as the discovery analysis. However there were never more than 12 vertices per category for which a solution was not found. Vertices were only excluded from analyses in situations where they clearly appeared as outliers, i.e. their presence changed the appearance of the contribution maps visualized on the surface. This was only the case for maps of the variability explained by the twin model. One vertex each was removed from the discovery SP and aFC variability map as well as from

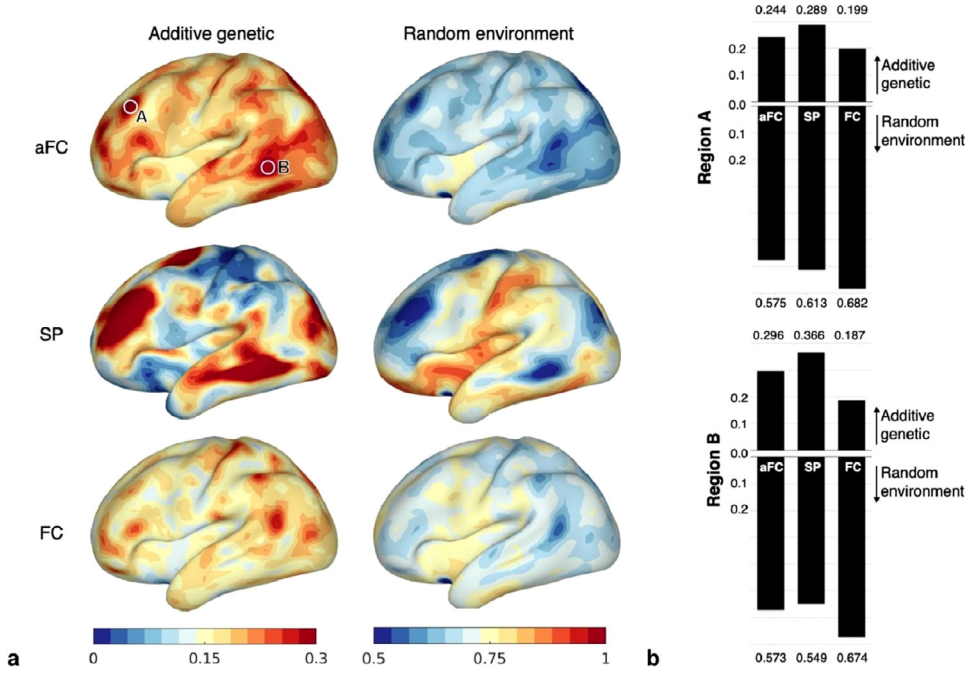

Fig. 2. Additive genetic and random environmental contribution to functional variability of the cortex. (a) After disentangling variability of spatial topography (SP) and connectivity strength (FC), SP exhibits pronounced peaks of genetic contribution of at least 30%, whereas the genetic contribution to FC mainly decreases compared to entangled functional variability (aFC). All values are positive and color maps are chosen to differentiate regions with high or low contribution. (b) For two regions of interest indicated in the aFC map, quantitative values are shown. Compared to aFC, genetic contribution is lower for FC and higher for SP. The contribution of random environment is highest for disentangled connectivity strength FC.

the FC variability map of the robustness analysis. As suggested by reviewers, a sensibility analysis by restricting the subjects to those with caucasian ancestry and using equal fractions of females for monozygotic and dizygotic twins was also performed.

3. Results

3.1. Divergent roles of genes and random environment in shaping strength and topography of networks

Genetic and common environmental contributions to aFC (A_{aFC} and E_{aFC}) were consistent with previous findings (Reineberg et al., 2019). For aFC, areas with low random contributions include the rostral middle frontal cortex, the pericalcarine cortex and the boundaries between temporal middle frontal inferior parietal cortex and superior temporal banks on both hemispheres, as well as two spots in the superior frontal cortex on the left hemisphere and one spot on the right hemisphere. The transverse temporal cortex, isthmus and several region boundary areas on the medial surface exhibit highest values of random contribution (Fig. 2). Surface maps for both hemispheres are provided in Supplementary Fig. 6. Genetic contribution ranges from 5.25 to 45.3% of the variance explained by the twin model.

After disentangling variability of function and spatial topography, genetic contributions to SP and FC diverge, and reveal a heterogeneous landscape across the cortex. In Fig. 2 two example regions at peaks of A_{aFC} illustrate this divergence, since A_{FC} decreases compared to A_{aFC} in both regions and A_{SP} increases. Random environmental contributions E_{SP} and E_{FC} show opposite behavour at least in region B. On average, genetic contribution to FC is lower compared to aFC (left hem: 19.3% (A_{aFC}) vs 16.5% (A_{FC}) of variance explained by genes, corrected p-value < 0.00001; right hem: 19% (A_{aFC}) vs 16.1% (A_{FC}) of variance explained by genes, corrected p-value < 0.00001, Fig. 3a). This decrease of genetic control is also apparent in Regions A and B in Fig. 2. The central sulcus is one of the few areas where local estimates of genetic contribution increased from A_{aFC} to A_{FC}. Random environment is the strongest influence on FC throughout the cortex with a lowest value of 45%, while genetic contribution ranges from 2.92 to 42%. In contrast to that, A_{SP} exhibits pronounced regional heterogeneity with genetic contribution accounting from 0% to 67% of the variance explained by the twin model, giving a mean genetic contribution of 15.53% of the variance explained on the left and 14.78% on the right hemisphere. In Region A and B in Fig. 2 the decrease from A_{aFC} to A_{FC} is mirrored by an increase from A_{aFC} to A_{SP}.

3.2. Two different gradients of genetic- and environmental influence on network strength and topography

We observed two different gradients in the genetic contribution to variability of connectivity strength and topography along an axis from primary areas to heteromodal networks. Fig. 3b shows the difference between A_{SP} and A_{FC} across the cortex. In primary areas, including visual- and somatomotor networks genetic contribution to functional connectivity strength variability A_{FC} dominates, while its contribution to topographical variability A_{SP} is comparably low. The opposite is the case in some regions belonging to higher-order areas, such as in frontoparietal areas, attention- and default mode networks (Yeo et al., 2011) where genetic contribution to A_{SP} is higher than A_{FC}. This coincides with a particularly high divergence between A_{SP} and $A_{FC,}$ and A_{SP} being at its peaks higher than E_{SP} (Supplementary Fig. 7). Those areas include parts of the rostral middle frontal, middle temporal and inferior parietal cortex on the left hemisphere, as well as at the boundary between the superior frontal and the precentral cortex. On the right hemisphere those areas include a part of the middle temporal cortex and an area along the boundary between superior frontal and caudal middle frontal cortex, reaching in the rostral middle frontal cortex. For 7 Yeo networks, visual- and somatomotor cortex exhibit predominantly areas with high A_{FC} / low A_{SP} paired with low E_{FC} / high E_{SP} (Fig. 3c). This divergence is reduced in dorsal- and ventral attention networks, and vanishes in fronto-parietal- and default mode networks. A robustness experiment shows that this observation is highly stable (Supplementary Fig. 8).

3.3. High genetic contribution to topography in more variable, and phylogenetically modern areas

We investigated the relationship of A_{SP} to network position variability (Nenning et al., 2017), the distance to primary areas and the amount of cortical expansion between macaque and human (Hill et al., 2010). A_{SP} correlates with variability (left hemi: $r = 0.3$, corrected p-value $=0.0054$; right hemi: $r = 0.41$, corrected p-value $=0.0054$ and cortical expansion from macaque to human (left: $r = 0.18$, corrected p-value 0.1044; right: $r = 0.099$, corrected p-value $= 0.3650$). The relationship between A_{SP} and the distance to primary area follows an inverted

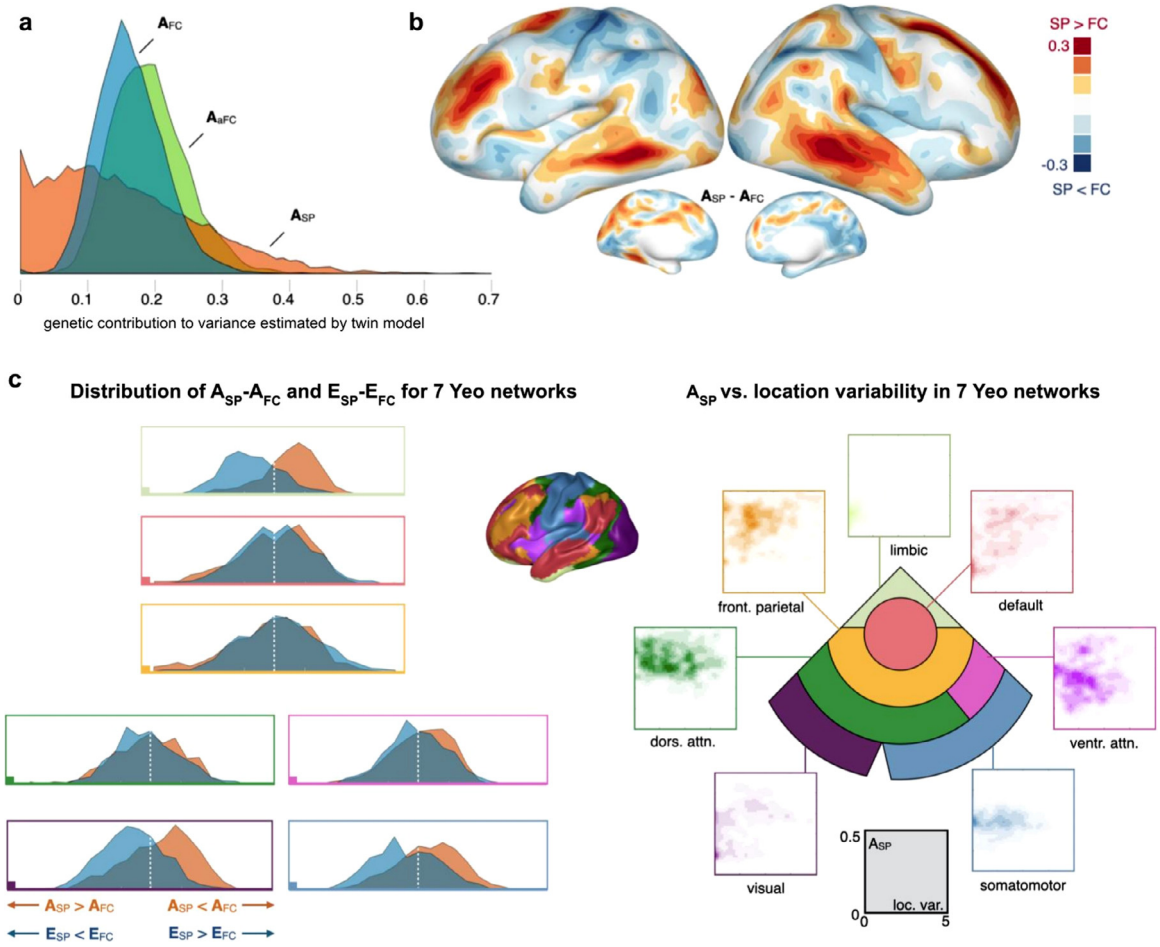

Fig. 3. Divergent roles of heritability for variability disentangled connectivity strength (FC) and spatial topography (SP) of function along a gradient from primary- to heteromodal areas. (a) Global distribution of additive genetic influence A for aFC, FC and SP. Compared to aFC, genetic contribution is smaller for FC, and exhibits a more heterogeneous landscape for SP. (b) Comparing genetic contribution to FC and SP across the cortex reveals areas of dominant influence on FC (visual- and somatomotor cortex) and areas of dominant influence on SP (attention-, fronto-parietal-, and default mode network) in 7 networks (Yeo et al. 2011). (c) Heritability of connectivity strength variability is most dominant in primary areas (visual, somatomotor) decreasing to a minimum in integration areas (frontoparietal, default mode). On the right, for each network, the distribution of location variability and genetic contribution is plotted.

U shape. It increases with distance to primary areas in somatomotor-, somatosensory-, visual cortex, dorsal and lateral attention network (left: r = 0.206, corrected p-value =0.2076; right: r = 0.286, corrected p-value = 0.1196), then decreases in limbic, fronto-parietal and default mode network (left: r = -0.275, corrected p-value = 0.1598; right: r = -0.01, corrected p-value = 0.5644). Supplementary Table 1 summarizes the values, and corrected as well as uncorrected p-values. Except variability, none of the correlations were significant after multi-comparisons correction. Fig. 4a shows the dominant high (red) or low (blue) A_{SP} in the space of location variance and the distance to the primary areas. This analysis reveals two *bands*: In low to medium areas there is a band of cortical regions exhibiting predominantly low A_{SP}. At the same time a diagonal band from areas with low variance close to the primary areas, to higher variance, and intermediate distance to primary areas exhibits predominantly high A_{SP}. Those areas include the middle temporal and the rostral middle frontal cortex on both hemispheres as well as parts of the superior frontal and inferior parietal cortex.

3.4. High genetic contribution to topography in areas in-between primary cortex and brain hubs

To further examine A_{SP} in the space of functional gradients spanning uni- to heteromodal, and task negative- to task positive networks, we plot high (red) or low (blue) A_{SP} dominance in the space spanned by the first, second and third functional gradients (Margulies et al., 2016) (Fig. 4b). In regions corresponding to association areas (high gradient 1), around visual processing (high gradient 2), and task positive activity (high gradient 3) high A_{SP} (red clusters) dominates locally, while in somatosensory and somatomotor areas (low gradient 1 and 2) low A_{SP} (blue cluster) dominates. Task negative areas (low gradient 3) exhibit a mixed composition without a clear dominant behavior with regard to A_{SP} (red and blue clusters). A *stream* of high (red) A_{SP} is situated along the edge from somatosensory/somatomotor to association areas through task positive regions. High genetic contributions modestly dominate the sparse central area of intermediate gradient 1 and 2.

3.5. Distinct strength and topography both contribute to overall variability

The overall variability as measured by the variance of connectivity strength before and after disentanglement estimated by the twin model is similar in magnitude (range aFC: 0.102 to 0.8, range FC: 0.105 to 0.76), and the genetic contributions A_{aFC} and A_{FC} moderately correlated on both hemispheres (left: r = 0.298, corrected p-value<0.00001; right: r = 0.273, corrected p-value<0.00001). The correlation between A_{aFC} and A_{SP} was 0.128 on the left and 0.198 on the right hemisphere (corrected p-value = 0. 0630 and corrected p-value = 0.005). Disentanglement of functional connectivity and topography reduces the correlation of genetic contributions to 0.05 (A_{FC} to A_{SP}) on the left- and 0.091 on the

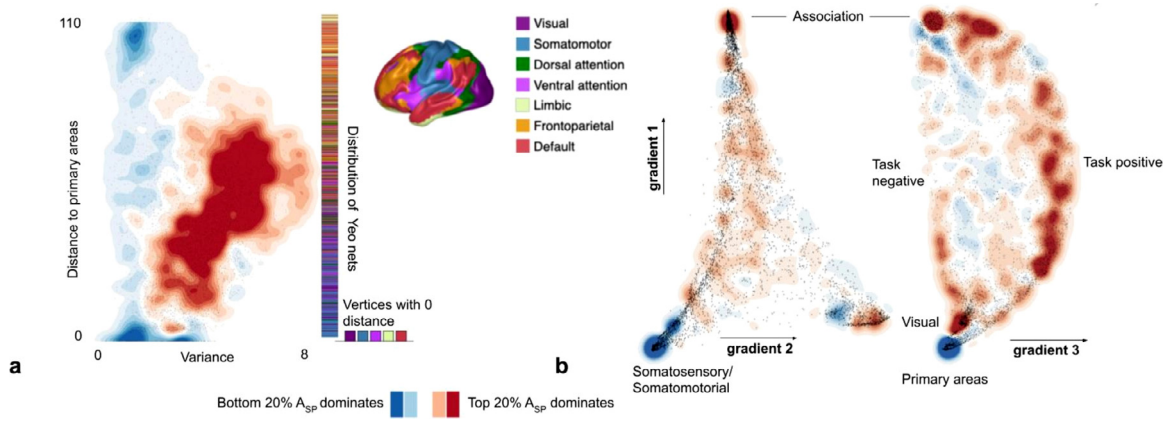

Fig. 4. Relationship of spatial variability and functional gradients to genetic contribution to spatial layout. (a) Areas where high- (top 20%) and low- (bottom 20%) A_{SP} dominate are plotted in a coordinate frame spanned by the variance of the spatial position of network areas and the distance to primary areas. (b) Analogously, A_{SP} dominance maps are visualized in the functional gradient space for gradients 1, 2, and 3 (Margulies et al. 2016). (For interpretation of the references to color in this figure, the reader is referred to the web version of this article.)

right hemisphere (corrected p-value=0.1336 and p-value=0.1056). The variability explained by the twin model for SP ranges from 7.98 mm^2 to 137 mm^2 when described as variance. This corresponds to a standard deviation ranging from 2.82 mm to 11.7 mm. Supplementary Table 2 summarizes correlations and their p-values. The hemispheres show similar patterns.

To gain a more detailed picture of the influence of FC and SP, we related their genetic contribution maps to cognitive functions, using a 12 component task activation model (Yeo et al., 2016) (Fig. 5). We were especially interested in comparing A_{SP} and A_{FC} in regions and corresponding functions, where both are high. Regions with high A_{FC} especially dominating over high A_{SP} are associated with visual processing and hand movements, whereas A_{SP} strongly dominates over A_{FC} in regions associated with inhibition and auditory processing.

3.6. Robustness and sensitivity analysis

We performed robustness analysis using 2 RL fMRI runs, available for each participant in addition to the 2 LR runs used for the main discovery analysis. In contrast to the LR runs, the phase encoding direction for the RL runs is from right to left (WU-Minn Consortium of the NIH Human Connectome Project, 2017), which might be a source of variance between runs of the same subject, in addition to the general intra-subject variance (Mueller et al., 2013;Cho et al., 2021). Disentangling resulted in comparable deformation fields of function and topography (Supplementary Fig. 3). SP, FC and aFC estimated by the twin model at each vertex correlate in the discovery- and robustness analysis (Supplementary Fig. 9). (aFC: left hemisphere: 0.98, right hemisphere: 0.98; FC: left: 0.93, right: 0.91; SP: left: 0.57, right: 0.65). The relationship between genetic and environmental influence, variability, as well as their distribution in the functional gradient space is highly replicable (Supplementary Fig. 10). Their respective dominance in 7 Yeo networks on the replication data, reflects those observed in the discovery data (Supplementary Fig. 8).

As suggested by the reviewers, we also conducted a sensibility analysis to rule out ancestry and gender as a potential confounder. We restricted our data to subjects with caucasian ancestry only and used the same fraction of females for monozygotic and dizygotic twins. Supplementary Fig. 11 shows the results of the sensibility analysis. Patterns generally stayed the same including heritability estimates of at least 0.3 for topographical variability at the temporal lobe and prefrontal cortex.

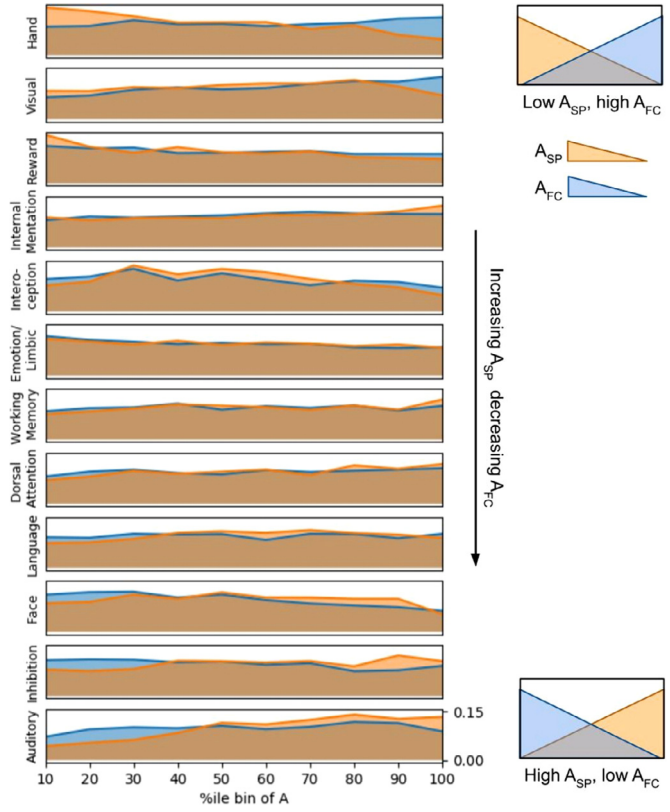

Fig. 5. Relation of genetic contribution to topographical variability and cognitive function. Values of A_{FC} and A_{PS} are divided into 10 bins based on percentiles (x-axis). Within each bin normalized activation probabilities are summed given one of 12 components (Yeo et al., 2016). The 12 components (rows) are ordered based on the difference of activation probabilities between A_{FC} and A_{PS} summed over bins and weighted by the log of percentile. The sequence visualizes the gradient from high A_{SP} and low A_{FC} on top, towards low A_{SP} and high A_{FC} on the bottom. (For interpretation of the references to color in this figure, the reader is referred to the web version of this article.).

4. Discussion

In this study we disentangled strength and topography of functional networks across the cortex. We applied a method to study the role of heritability and individual experience shaping these two key features

independently. Disentanglement revealed that their influence on variability of strength and topography diverges across the cortex. While in primary areas, variability of strength is more heritable compared to topography, the opposite is the case in areas belonging to intermediate and higher order association areas. There, genetic factors primarily shape variability of topography, while variability of connectivity strength is predominantly determined by individual experience. Our results may inform our understanding of the mechanisms of emergence and continued adaptation of brain areas unique to humans.

4.1. Variable and heritable topography in intermediate and higher order association areas

In evolutionary older parts of the cortex, functional connectivity is related to proximity (Sepulcre et al., 2010). The modern human association cortex does not follow this rule anymore. The *tethering hypothesis* (Buckner and Krienen, 2013) posits that regions that form modern association cortex became untethered from strong patterning signals of thalamic input in the past due to cortical expansion. This fostered a less hierarchical connectivity landscape in these regions. Together with an increase in cortico-cortical connectivity and their position between signal gradients from distributed primary areas, this may have paved the way for being subsequently co-opted for high-level integrative cognitive capabilities. In light of this, the rapid evolutionary expansion of association cortex may also have led to a dissociation between the roles of functional components and their spatial layout, contributing to the high variability these networks exhibit compared to primary areas (Mueller et al., 2013; Sepulcre et al., 2010; Buckner and Krienen, 2013). The precise role of this variability is, however, not clear.

We did observe dissociation of genetic influences on the variability of strength and topography in association cortex. While here, topography and connectivity strength are highly variable, the variability of the first is heritable to a much higher degree than the latter. Therefore the development of a less hierarchical connectivity landscape may have gone along with an increase in genetic variability encoding topographical variability. Since the genetic variability is still present today, different genotypes may have formed the basis of equally fit phenotypes in the past. At the same time, genetic influence may enable improving a coordinated - and eventually possibly even canonical - layout of processing pathways in the future, as heritability renders topographic variability visible to selection and adaptation, enabling the emergence of replicable organization. At the same time, the strength of the interconnectedness among the components anchored in a diverse, but heritable landscape is shaped by individual experience and the environment.

The observation that highly variable, and heritable topography overlaps in association cortex, is initially counterintuitive, but may have benefits on the individual-, and the population level. It may afford connectivity strength's variability and susceptibility to random environmental influence on top of an underlying coordinated framework of network topography, necessary for the acquisition of higher-order human cognitive abilities. At the same time, on the population level, simultaneous variability and heritability of topography may not only be a transient state while organization is optimizing, but instead a means to sustain population level diversity and fitness (Amy and Bauernfeind, 2019). For either point, the separation of variability explained by heritable traits versus random environmental influence and their independent link to topography and connectivity strength are important.

4.2. Coordinated processing pathways from primary to heteromodal areas

An increase of heritable topographical variability from visual and somatomotor cortex to default and fronto-pariental networks (Fig. 3c) supports the two hypotheses regarding different but coordinated heritable integration pathways. Task positive areas of high genetic contribution are in close proximity of early to intermediate processing areas found in a study of pathways from primary areas to network hubs (Sepulcre et al., 2012). When taking into account areas whose variability is influenced by common environment, low random contribution areas are next to the dorsolateral prefrontal cortex (DLPFC), the frontal eye fields (FEF) and a stream following the borders of the visual cortex to the lateral occipitotemporal junction (LOTJ) and then reaching into task-negative areas of the temporal lobe. Early integration areas of the visual processing stream form a cluster of high genetic contribution to SP present in the visual cortex in Fig. 4b. The visual cortex' connectivity follows three pathways (Sepulcre et al., 2012), a feature not present for the other primary cortices. Genetic coding of network position variability in the visual cortex may be needed to robustly sustain a more intricate pathway structure. The low genetic contribution to topographical variability A_{SP} in somatosensory and somatomotor areas might be a consequence of the low variability SP in these areas which can be seen in Fig. 4a. It suggests that the topography of these regions is already quite settled and therefore under tight genetic control, while this is not the case for the remaining observed topographical variability.

Low to intermediate integration areas exhibit comparably high heritability of functional connectivity strength variability (FC), though to a lesser extent. Peak areas are close to LOTJ and DLPFC, two regions belonging to integration areas not directly adjacent to the somatomotor and somatosensory cortex, and in case of the DLPFC not adjacent to the visual cortex (Sepulcre et al., 2012). The stronger genetic encoding of connectivity strength variability in these areas might be necessary to effectively bridge the larger distance compared to areas located directly next to primary areas.

4.3. Disentanglement sheds new light on heritability of entangled functional connectivity strength

The entire cortex shows moderate genetic influence on connectivity strength variability before disentanglement (aFC). Disentangling FC and SP reveals a predominantly decreased A_{FC} compared to A_{aFC} and a location dependent increase of A_{SP}. This suggests that genetic influence on aFC to a relevant extent actually reflects A_{SP}. Further evidence on that is provided in a recent study distinguishing connectivity profiles of sibling pairs from pairs of unrelated individuals (Miranda-Dominguez et al., 2018). Although the study did not investigate heritability of topography directly, the authors used a parcellation to obtain regions of interest (ROIs) and described the time series of each ROI by the time series of all other ROIs through regression. They then used the obtained coefficients as a connectivity profile of a ROI. Most areas of low random environmental contribution to spatial topography overlap with cortical regions among the top 20 to distinguish sibling pairs from pairs of unrelated individuals (Miranda-Dominguez et al., 2018) (Supplementary Fig. 12), suggesting that part of aFC and the corresponding additive genetic contribution is actually due to variability of the spatial layout of functional units on the cortex.

This complements our emerging understanding of the role of variability of brain networks. As found in a recent study, variability in overall functional connectivity is actually reflected in the variability of topographical organization and the spatial arrangement of functional regions strongly predicts behavior (Bijsterbosch et al., 2018). In another recent study (Kong et al., 2019) the entire cortical parcellation based on network topography was able to predict measures of cognition, personality and emotion. Together with our findings this suggests that different behavioral traits might be genetically determined through topography and have been either equally advantageous under similar conditions or alternatingly advantageous under changing conditions during human evolution.

Even though A_{SP} seems to determine A_{aFC} for some parts of the cortex, A_{FC} also has its role when looking at specific cognitive functions. Whereas genetic influence on most cognitive functions can be attributed to a mixture of A_{SP} and A_{FC} without a clear dominance of one of the two, there are also some exceptions as indicated by differences in ranking in Fig. 5. Dorsal attention and language seem to be influenced geneti-

cally mainly through SP, since those functions are ranked at the bottom. Visual and hand movement related processing, on the other hand, are influenced genetically mainly through FC.

4.4. Related work

A range of papers has investigated genetic determination of morphology (White et al., 2002; Chen et al., 2011) as well as structural (Shen et al., 2014; Xie et al., 2018) and functional features of the brain (Glahn et al., 2010; Reineberg et al., 2019; Colclough et al., 2017; Miranda-Dominguez et al., 2018). In a study of White et al. (2002) cerebral brain volumes of twins, including whole brain volume as well as divisions into lobes and tissue types, showed correlations above 0.90, except the frontal white matter and occipital gray matter volume. Genetic correlations for surface area with different seed locations have been explored in Chen et al. (2011) and showed an anterior-posterior division and a lack of long distance correlations. Similar to surface area, cortical thickness exhibited local genetic correlation with additional strong genetic correlation to homologs on the opposite hemisphere in another study (Alexander-Bloch et al., 2019). Glahn et al. (2010) explored heritability of anatomical morphology and functional aspects of the default mode network, revealing an independent genetic influence on anatomical morphology and functional variability. Some other previous studies based on fMRI data used a univariate twin model to investigate the connectivity of single edges between regions distributed across the cortex (Reineberg et al., 2019; Colclough et al., 2017). Observed genetic contributions are higher than common environmental influences in both papers. A multivariate machine learning based approach was used in Miranda-Dominguez et al. (2018) to distinguish sibling pairs from pairs of unrelated individuals. Useful regions for pair classification belonged to higher order systems, such as the fronto-parietal, dorsal attention and default mode network. Measures of structural connectivity were found to be especially heritable for connections within the default mode network, visual circuits and connections between default mode and fronto-parietal or ventral attention network (Shen et al., 2014; Xie et al., 2018).

4.5. Limitations

This study has several limitations. One limitation is the way how the genetic, common environmental and random environmental contributions to connectivity strength at each vertex are estimated. Since the brain is a network, describing the connectivity strength or profile of each vertex should preferably be done by including the connections to all nodes in the brain. However, due to the large number of parameters which had to be estimated for the twin model, this option is computationally infeasible. Therefore we describe the connectivity profile of each vertex by its connectivity to predefined regions of interest, an approach consistent with prior work (Yeo et al., 2011). A limitation of the twin model used is that it only models contributions that act additively on the inter-subject variability. Including interactions of genetic and environmental influences in the model could give additional insights. Further limitations are that the power to separate A from C is lower than for separating A from E, which can lead to the partial attribution of common environmental influence to genetic influence or vice-versa. We also found significant correlations between test-retest reliability and heritability for FC (left corr=0.3024, corrected p-value < 0.00001; right corr=0.3000, corrected p-value < 0.00001) and SP (left corr =0.3674, corrected p-value = 0.0046; right corr= 0.4545, corrected p-value=0.0049). However, heritability is not completely explained by test-retest reliability. This is also suggested by a much higher correlation of test-retest reliability of SP and FC (0.532, both hemispheres) compared to the correlation between heritability of FC and SP (0.072, both hemispheres). We also show brain maps where we regressed out 1-test-retest variability in Supplementary Fig. 14. Concerns of reliability have also been addressed through robustness analysis, which showed that the main findings are stable across runs and suggests that the processing stream from unimodal to heteromodal areas shows an interplay of rather genetically determined topography and functional connectivity strength determined rather by random environment, which deserves more investigation in the future.

Declaration of Competing Interest

None

Credit authorship contribution statement

Bianca Burger: Software, Formal analysis, Writing – original draft, Writing – review & editing, Visualization. **Karl-Heinz Nenning:** Writing – review & editing. **Ernst Schwartz:** Writing – review & editing. **Daniel S. Margulies:** Writing – original draft, Writing – review & editing. **Alexandros Goulas:** Writing – review & editing. **Hesheng Liu:** Resources, Writing – review & editing. **Simon Neubauer:** Writing – original draft, Writing – review & editing. **Justin Dauwels:** Writing – review & editing. **Daniela Prayer:** Writing – review & editing. **Georg Langs:** Conceptualization, Writing – original draft, Writing – review & editing, Visualization, Supervision.

Acknowledgements

We thank Oscar Miranda-Dominguez for sharing his version of the Gordon parcellation with us. This work was supported by the Medical University of Vienna, the Austrian Research Fund (FWF) [grants P 35189, P 34198, and I 3925-B27] in collaboration with the French National Research Agency (ANR), the Vienna Science and Technology Fund (WWTF) [LS20-065], the European Research Council Grant [866533-CORTIGRAD], the National Natural Science Foundation of China [Grant No. 81790652, No.81790650] and the NAM Advanced Biomedical Imaging Program [FY2016] between Nanyang Technological University, Singapore and Medical University of Vienna, Austria.

Data and code availability

Third party code used in this study included Connectome Workbench v1.3[26] (https://github.com/Washington-University/workbench/releases/tag/v1.3.2) and Freesurfer v5.3[25] (https://surfer.nmr.mgh.harvard.edu/fswiki/DownloadAndInstall5.3) for preprocessing and MSM v2[30–32] (https://www.doc.ic.ac.uk/~ecr05/MSM_HOCR_v2/) and mapalign (https://github.com/satra/mapalign) for functional alignment. Own code was developed in R 3.4 for setting up the twin model using R's package OpenMx version 2.11.5 (Bürger, 2000; Neale et al., 2016; Hunter, 2018) (https://openmx.ssri.psu.edu/), as well as in Python 3.6 for calculation of connectivity matrices. Matlab 2018 was used for generation of figures and the spin test (https://www.github.com/spin-test). Code and data generated during this study is publicly available on Github (https://github.com/cirmuw/functional-twin-analysis).

Supplementary materials

Supplementary material associated with this article can be found, in the online version, at doi:10.1016/j.neuroimage.2021.118770.

References

Alexander-Bloch, A.F., et al., 2018. On testing for spatial correspondence between maps of human brain structure and function. Neuroimage 178, 540–551.
Alexander-Bloch, A.F., et al., 2019. Human cortical thickness organized into genetically-determined communities across spatial resolutions. Cereb. Cortex 29, 106–118.
Amy, L., Bauernfeind, C.C.B., et al., 2019. Genetic diversity underlying behavioral plasticity in human adaptation. In: Bear, M., et al. (Eds.), Evolution of the Human Brain: From Matter to Mind. Elsevier B.V., pp. 41–65 vol. 250.

Bijsterbosch, J.D., et al., 2018. The relationship between spatial configuration and functional connectivity of brain regions. Elife 7.
Buckner, R.L., Krienen, F.M., 2013. The evolution of distributed association networks in the human brain. Trends Cogn. Sci. doi:10.1016/j.tics.2013.09.017.
Bürger, R., 2000. The Mathematical Theory of Selection, Recombination, and Mutation. Wiley.
Chen, C.H., et al., 2011. Genetic influences on cortical regionalization in the human brain. Neuron 72, 537–544.
Cho, J.W., Korchmaros, A., Vogelstein, J.T., Milham, M., Xu, T, 2021. Impact of concatenating fMRI Data on reliability for functional connectomics. Neuroimage 226.
Coifman, R.R., Lafon, S., 2006. Diffusion maps. Appl. Comput. Harmon. Anal. 21, 5–30.
Colclough, G.L., et al., 2017. The heritability of multi-modal connectivity in human brain activity. Elife 6.
Dubois, J., Galdi, P., Han, Y., Paul, L.K., Adolphs, R., 2018. Resting-state functional brain connectivity best predicts the personality dimension of openness to experience. Personal Neurosci. 1.
Fischl, B., Sereno, M.I., Tootell, R.B., Dale, A.M, 1999. High-resolution intersubject averaging and a coordinate system for the cortical surface. Hum. Brain Mapp. 8, 272–284.
Glahn, D.C., et al., 2010. Genetic control over the resting brain. Proc. Natl. Acad. Sci. U. S. A. 107, 1223–1228.
Glasser, M.F., et al., 2013. The minimal preprocessing pipelines for the Human Connectome Project. Neuroimage 80, 105–124.
Glasser, M.F., et al., 2016. A multi-modal parcellation of human cerebral cortex. Nature 536, 171–178.
Griffanti, L., et al., 2014. ICA-based artefact removal and accelerated fMRI acquisition for improved resting state network imaging. Neuroimage 95, 232–247.
Gunz, P., et al., 2009. Early modern human diversity suggests subdivided population structure and a complex out-of-Africa scenario. Proc. Natl. Acad. Sci. 106, 6094–6098.
Gunz, P., et al., 2019. Neandertal introgression sheds light on modern human endocranial globularity. Curr. Biol. 29, 895.
Gunz, P., Neubauer, S., Maureille, B., Hublin, J.J., 2010. Brain development after birth differs between Neanderthals and modern humans. Curr. Biol. 20, R921–R922.
Hill, J., et al., 2010. Similar patterns of cortical expansion during human development and evolution. Proc. Natl. Acad. Sci. U. S. A. 107, 13135–13140.
Hunter, M.D., 2018. State space modeling in an open source, modular, structural equation modeling environment. Struct. Equ. Model. A Multidiscip. J. 25, 307–324.
Ishikawa, H., 2014. Higher-order clique reduction without auxiliary variables. In: Proceedings of the IEEE Conference on Computer Vision and Pattern Recognition doi:10.1109/cvpr.2014.177.
Kong, R., et al., 2019. Spatial topography of individual-specific cortical networks predicts human cognition, personality, and emotion. Cereb. Cortex 29, 2533–2551.
Krubitzer, L.A., Prescott, T.J., 2018. The Combinatorial creature: cortical phenotypes within and across lifetimes. Trends Neurosci. 41, 744–762.
Langs, G., et al., 2014. Decoupling function and anatomy in atlases of functional connectivity patterns: language mapping in tumor patients. Neuroimage 103, 462–475.
Marcus, D.S., et al., 2013. Human Connectome Project informatics: quality control, database services, and data visualization. Neuroimage 80, 202–219.
Margulies, D.S., et al., 2016. Situating the default-mode network along a principal gradient of macroscale cortical organization. Proc. Natl. Acad. Sci. U. S. A. 113, 12574–12579.
Miranda-Dominguez, O., et al., 2018. Heritability of the human connectome: a connectotyping study. Netw. Neurosci. 2, 175–199.
Mueller, S., et al., 2013. Individual variability in functional connectivity architecture of the human brain. Neuron 77, 586–595.
Neale, M.C., et al., 2016. OpenMx 2.0: extended structural equation and statistical modeling. Psychometrika 81, 535–549.
Neale, M.C., Maes, H.H.M., 2021. Methodology For Genetic Studies of Twins and Families (pp.177-200). Kluwer Academic Publishers B.V..
Nenning, K.H., et al., 2017. Diffeomorphic functional brain surface alignment: functional demons. Neuroimage 156, 456–465.
Nenning, K.H., Kollndorfer, K., Schöpf, V., Prayer, D., Langs, G., 2015. Multi-subject manifold alignment of functional network structures via joint diagonalization. Inf. Process. Med. Imaging 24, 462–473.
Neubauer, S., Gunz, P., Hublin, J.J., 2010. Endocranial shape changes during growth in chimpanzees and humans: a morphometric analysis of unique and shared aspects. J. Hum. Evol. 59, 555–566.
Neubauer, S., Hublin, J.J., Gunz, P., 2018. The evolution of modern human brain shape. Sci. Adv. 4, eaao5961.
Reineberg, A.E., Hatoum, A.S., Hewitt, J.K., Banich, M.T., Friedman, N.P., 2019. Genetic and environmental influence on the human functional connectome. Cereb. Cortex doi:10.1093/cercor/bhz225.
Robinson, E.C., et al., 2014. MSM: a new flexible framework for multimodal surface matching. Neuroimage 100, 414–426.
Robinson, E.C., et al., 2018. Multimodal surface matching with higher-order smoothness constraints. Neuroimage 167, 453–465.
Salimi-Khorshidi, G., et al., 2014. Automatic denoising of functional MRI data: combining independent component analysis and hierarchical fusion of classifiers. Neuroimage 90, 449–468.
Schaefer, A., et al., 2018. Local-global parcellation of the human cerebral cortex from intrinsic functional connectivity MRI. Cereb. Cortex 28, 3095–3114.
Seghier, M.L., Price, C.J, 2018. Interpreting and utilising intersubject variability in brain function. Trends Cogn. Sci. 22, 517–530.
Sepulcre, J., et al., 2010. The organization of local and distant functional connectivity in the human brain. PLoS Comput. Biol. 6, e1000808.
Sepulcre, J., Sabuncu, M.R., Yeo, T.B., Liu, H., Johnson, K.A, 2012. Stepwise connectivity of the modal cortex reveals the multimodal organization of the human brain. J. Neurosci. 32, 10649–10661.
Shen, K.K., et al., 2014. Investigating brain connectivity heritability in a twin study using diffusion imaging data. Neuroimage 100, 628–641.
Smaers, J.B., Soligo, C., 2013. Brain reorganization, not relative brain size, primarily characterizes anthropoid brain evolution. Proc. R. Soc. B Biol. Sci. 280.
Stoecklein, S., et al., 2020. Variable functional connectivity architecture of the preterm human brain: impact of developmental cortical expansion and maturation. Proc. Natl. Acad. Sci. U. S. A. 117, 1201–1206.
Uğurbil, K., et al., 2013. Pushing spatial and temporal resolution for functional and diffusion MRI in the human connectome project. Neuroimage 80, 80–104.
Van Essen, D.C., et al., 2012. The human connectome project: a data acquisition perspective. Neuroimage 62, 2222–2231.
Van Essen, D.C., et al., 2013. The WU-Minn human connectome project: an overview. Neuroimage 80, 62–79.
White, T., Andreasen, N.C., Nopoulos, P., 2002. Brain volumes and surface morphology in monozygotic twins. Cereb. Cortex 12, 486–493.
WU-Minn Consortium of the NIH Human Connectome Project. 1200 subjects reference manual – appendix I. https://humanconnectome.org (2017).
Xie, L., et al., 2018. Heritability estimation of reliable connectomic features. Connect Neuroimaging 11083, 58–66 (2018).
Yeo, B.T.T., et al., 2011. The organization of the human cerebral cortex estimated by intrinsic functional connectivity. J. Neurophysiol. 106, 1125–1165.
Yeo, B.T.T., et al., 2016. Functional specialization and flexibility in human association cortex. Cereb. Cortex 26, 465.